8

Microscopic examination of deteriorated concrete

T. G. NIJLAND and J. A. LARBI[1],
TNO Built Environment and Geosciences, The Netherlands

Abstract: Concrete petrography is the integrated microscopic and mesoscale (hand specimen size) investigation of hardened concrete, that can provide information on the composition of concrete, the original relationships between the concrete's various constituents, and any changes therein, whether as a result of ageing or damage processes. Concrete petrography itself may serve different purposes, such as product evaluation and control, determination of the type of aggregate or binder used, and damage diagnosis. This chapter aims to introduce engineers and material scientists to concrete petrography as a useful investigative tool or technique to assess concrete in structures.

Key words: concrete, petrography, microscopy, damage diagnosis.

8.1 Introduction

Concrete petrography is the integrated microscopic and mesoscale (hand specimen size) investigation of hardened concrete, that can provide information on the composition of concrete, the original relationships between the concrete's various constituents, and any changes therein, whether as a result of ageing or damage processes. A thin section of concrete prepared from a core or sample is studied under the microscope. This thin section is so thin that one can see through the constituents. Concrete petrography is not a non-destructive technique in the strict sense of the word. However, as the amount and size of samples required to obtain a great wealth of information is very small compared with the structure itself, concrete petrography can be regarded as a very minor intrusive technique.

Concrete petrography itself may serve different purposes, such as product evaluation and control, determination of the kind of aggregate or binder used, determining quantitative composition of hardened concrete (whether or not in combination with chemical analysis), evaluating the extent of mixing and compaction and damage diagnosis. Damage diagnosis may

[1]Deceased, June 13, 2009.

range from construction errors or flaws to physical attack, such as the effects of freeze–thaw cycles, and chemical attack such as sulfate attack in the form of delayed ettringite formation (DEF) or destructive thaumasite formation and alkali–aggregate reactions such as alkali–silica reaction (ASR) and alkali–carbonate reaction (ACR). Petrographic investigation might even be extended to the early, non-hardened phase of concrete, by use of the so-called 'active thin sections' (De Rooij and Bijen 1999, De Rooij *et al*. 1999). Besides application to cement-based concretes, petrography may also be applied to other building materials such as masonry mortars (Larbi 2004), glazed tiles (Larbi 1997), refractories (Rossikhina *et al*. 2007), or sulfur concrete (Jakobsen 1990).

Microscopic investigation of concrete finds its roots in the geological discipline of petrography and petrology, the study of the origin and evolution of natural rocks. This study was greatly enhanced by the development of the petrographic or polarizing microscope during the first half of the 19th century by a small group of British scientists, in particular Davy, Brewster, Nicol and Sorby. The polarizing microscope enabled identification of minerals in rocks by determining physical or optical properties of minerals such as relative refractive indices, birefringence, pleochroism, and optical orientation. This identification is the basis for studying mutual original relationships (texture, microstructure), in order to unravel various genetic processes, and subsequent changes, resulting from metamorphism, weathering and any damaging processes, such as alkali–aggregate reactions and sulfate attack in concrete.

Refractive indices (or indices of refraction) are a measure of how the velocity of light through a crystal (or other medium) is reduced compared with the velocity of light in vacuum; the refractive index n = light velocity in vacuum/light velocity in a crystal.

Birefringence is the difference between the most divergent, i.e. smallest and largest, refractive indices of a crystalline phase, manifest as an interference colour in cross-polarized light; if a crystal has perfect (cubic) symmetry, the birefringence is zero and the crystal remains black under cross-polarized light in all directions.

Pleochroism is the property of a crystal exhibiting different colours because the crystal structure absorbs a particular wavelength depending on the direction of vibration light passing through a crystal.

Optical orientation is the orientation of the optical indicatrix, i.e. the mathematical surface of light rays moving through a phase in all directions, relative to a mineral's crystallographic axis.

Microscopic investigation of concrete has been around for over a century, if one allows for the early microscopic investigation of Portland cement clinker as the birth of concrete petrography. From 1882 onwards, the French scientist Henry le Chatelier studied the hardening of Portland cement, cumulating in his thesis *'Recherches expérimentales sur la constitution des mortiers hydrauliques'*, submitted in 1887. Using methods developed by Henry Clifton Sorby (1826–1908), who developed the making of thin sections of rocks and minerals and demonstrated the application of the polarizing microscope to study them (Sorby 1858), Le Chatelier studied Portland cement clinker using a polarizing microscope and identified the phases tri- and dicalcium silicate, C_3S and C_2S, (and/or their impure analogues alite and belite) tricalcium aluminate, C_3A and tetracalcium aluminoferrite C_4AF (Desch 1938). Polarizing microscopy subsequently became a production control tool for cement plants, first applied by the Swedish geologist Törnebohm (1897), and greatly enhanced by the works of Yoshio Ono of Onoda Cement Company in Japan over the second half of the 20th century (Campbell 2004).

Concrete petrography developed as a separate discipline. Microscopy on concrete as an entity rather than its components was already applied by Johnson (1915), using reflective light microscopy. However, concrete petrography in the present day sense was prompted by Stanton's discovery of the alkali–silica reaction in 1940. Soon afterwards, microscopic studies of deteriorated concrete and aggregates followed (e.g. Hansen 1944, Parsons and Ingsley 1948). Concrete petrography developed alongside the petrographic evaluation of aggregates intended for use in concrete (e.g. ASTM C295 1954, Dolar-Mantuani 1983). In the 1960s, concrete petrography by means of polarization microscopy had been developed to such an extent, that the first reviews were published (e.g. Mielenz 1962, Mather 1965). Later, polarization microscopy was supplemented with fluorescence methods by B. Romer and G. Dubrolubov (Jana 2005), to become polarizing-and-fluorescence microscopy (PFM). More recently, a review of concrete petrography has been given by French (1991) and a full text book was provided by St. John *et al*. (1998). The present contribution does not aim to duplicate previous works, but aims to introduce engineers and material scientists to concrete petrography as a useful investigative tool or technique to assess concrete in structures.

8.2 A concise approach

Concrete petrography is aimed at answering three questions, viz.:

- Which components or constituents are present in the concrete specimen (Fig. 8.1)? Type of cement, aggregate, water (visible as water-binder ratio), and other components or constituents.

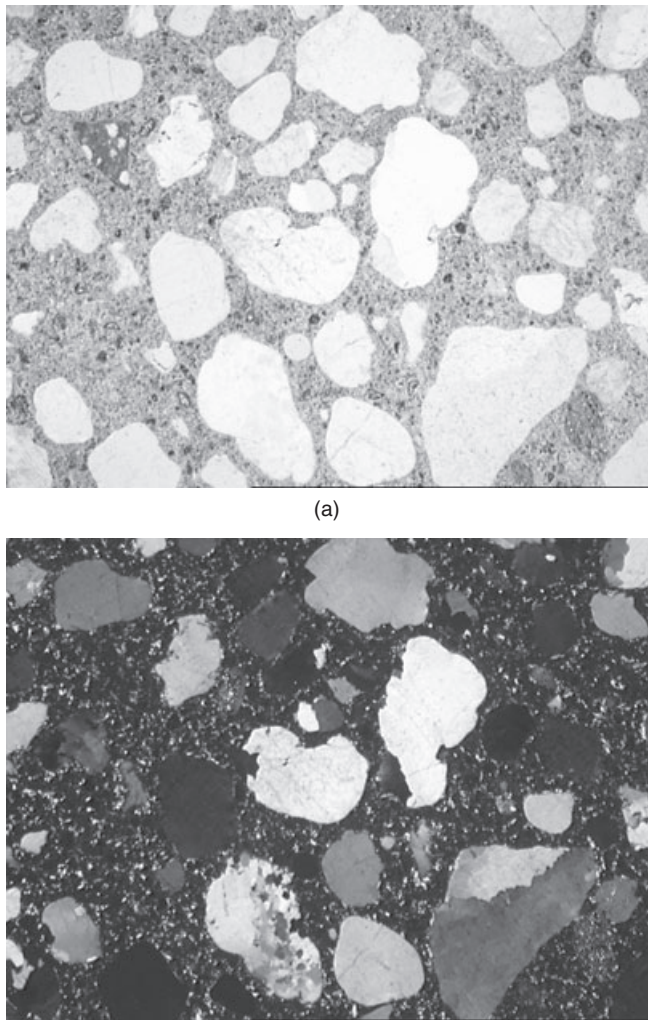

(a)

(b)

8.1 Microphotograph showing a typical example of concrete microstructure comprising cement paste, aggregate, and air voids, (a) in plane polarized light, (b) in cross polarized light (view 5.4 mm × 3.5 mm).

- What are the mutual relations between the various components? Microstructure of binder, distribution of aggregate, mutual interface, and interactions of the various constituents with each other.
- What observations point towards changes in the concrete? Extent of microcracking (Fig. 8.2), formation of new, secondary phases, and evidence of deterioration or attack and its effect on the concrete.

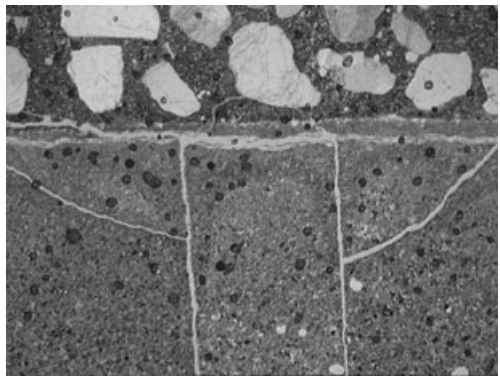

8.2 Example of microcracks: microphotograph showing cracking in injection grout (plane polarized light, view 5.4 mm × 3.5 mm).

To interpret the foregoing aspects requires a combination of basic petrographic identification techniques, knowledge of cement chemistry, familiarity with concrete technology and building practice, as well as mechanisms of concrete deterioration. A good introduction to optical crystallography, as a basis for optical mineral identification, is given by Bloss (1994), whereas both Taylor (1998) and Hewlett (1998) provide a wealth of background information on cement and concrete chemistry. Table 8.1 and Fig. 8.3 give an overview of some optical properties of Portland cement clinker phases, hydration products and relevant natural analogues and secondary phases. In identifying primary aggregates, the book series by MacKenzie and coworkers (Adams *et al*. 1984, MacKenzie *et al*. 1982, Yardley *et al*. 1990) may be useful. Relevant information on concrete technology may be found in, for example, Addis and Owens (2001) and Neville and Brooks (2001). When examining historic concretes, it might be useful to appreciate the state of knowledge at the time of building. Reference works of that time, such as Eckel (1928), might be quite useful.

Petrographic analysis of deteriorated concrete involves a series of stages, starting with sampling macroscale, and ending with the concrete's microscopic or even submicroscopic investigation. Generalizing, any petrographic analysis will include:

- A well-designed sampling strategy, both on macro- and mesoscale, depending on the structure and damage features. Sampling should provide a basis for assessing the condition of a structure as a whole (macroscale), and specific location of thin sections to be made from a hand specimen or core (mesocale) should be determined in order to be sure that relevant processes or phenomena might be observed in the thin section.

Table 8.1 Compilation of optical data for Portland cement clinker phases, hydration products and relevant natural analogues, and secondary phases. Abbreviations: n_α or n_ε is the smallest refractive index for optically unixial or biaxial phases, respectively; n_β is the intermediate refractive index for optically biaxial phases; n_γ or n_ω is the largest refractive index for optically unixial or biaxial phases, respectively; Δ is the birefringence; $2V$ is the angle between the optical axes; Disp. is the dispersion of the optical axes; and L′ is the elongation

Phase			n_α or n_ε	n_β	n_γ or n_ω	Δ	$2V$	Disp.	L′	Reference
Alite-T1, pure	C_3S	Triclinic	1.7139		1.7172	0.0033				1,2
Alite-T1, typical clinker	C_3S	Triclinic	1.7158–1.7197		1.7220–1.7238	0.0041–0.0062				1,2
Aluminosulfate		Cubic		1.569		Isotropic				2
Anhydrite		Orthorhombic	1.5698	1.5754	1.6136	0.0438	+43	$r < v$		2
			1.5700	1.5757	1.6138	0.0438	+42			3
Bassanite		Hexagonal	1.505		1.548	0.043	+0			2
Belite-α, bredigite	C_2S		1.713	1.717	1.732	0.019	+20–30			1
Belite-β, synthetic	C_2S	Monoclinic	1.717		1.735	0.018	+Large			2
Belite-β, larnite	C_2S	Monoclinic	1.707	1.715	1.730	0.023	+70–75			3
Belite-γ	C_2S	Orthorhombic	1.642	1.645	1.654	0.012	+60			2
Blast-furnace slag		Amorphic				Isotropic				
Brucite		Trigonal	1.581		1.561	0.020	Anomalous, small	$r >> v$	–	2
			1.580–1.581		1.559–1.566	0.015–0.021				3
Calcite		Trigonal	1.486		1.658	0.1719	<25			3
Calcium langbeinite		Orthorhombic	1.522	1.526	1.527	0.005	Small			2
C-S-H			Mean 1.603						+	5
Dicalcium aluminate	C_2A	Monoclinic	1.6178	1.6184	1.6516	0.0338	+12			2
Dicalcium silicate hydrate-α	C_2SH	Orthorhombic	1.614 ± 0.002	1.620 ± 0.002	1.633 ± 0.002	0.019	+68		+	1

Dicalcium silicate hydrate-β, Hillebrandite	C_2SH	Monoclinic	1.605 ± 0.005		1.6012 ± 0.003	0.005–0.009	60–80	*v* >> *r*	1
Ettringite		Trigonal	1.459		1.463	0.004	0		2
			1.4618		1.4655	0.0037	0		4
Ferrite, brownmillerite	C_4AF	Orthorhombic	1.96	2.01	2.04	0.09	Mod.	+	2
			1.98	2.05	2.08	0.10	Mod.		6
Gypsum		Monoclinic	1.5205	1.5226	1.5296	0.0091	+58	±	2,3
Hemihydrate, 0.5 H_2O		Monoclinic	1.559	1.5595	1.5836	0.0246	+14		2
Hemihydrate, 0.8 H_2O		Trigonal	*c.* 1.56		*c.* 1.59	*c.* 0.03	+		2
Hydrocalumite		Monoclinic	1.535	1.553	1.557	0.022	24		4
Hydrogarnet		Cubic		1.671–1.681		Isotropic, weakly birefringent			3,4
Hydrotalcite		Trigonal	1.494–1.504		1.510–1.518	0.012–0.017	0		4
Jennite		Triclinic	1.552 ± 0.003	1.564 ± 0.003	1.571 ± 0.003	0.019	74		5
Monocalcium aluminate		Monoclinic	1.643	1.655	1.633	0.010	36		2
Monosulfate, Al-rich	Afm		1.49–1.54		1.50–1.56	0.01–0.07			2
Monosulfate, Fe^{3+}-rich	Afm		1.54–1.60		1.56–1.61	0.02–0.07			2
Periclase		Cubic		1.730–1.739		Isotropic			3,4
Pleochroite		Orthorhombic	1.669		1.673–1.680	0.004–0.011	+45		6

Table 8.1 Continued

Phase			n_α or n_ε	n_β	n_γ or n_ω	Δ	$2V$	Disp.	L′	Reference
Portlandite		Hexagonal	1.545		1.573	0.028	0			2
			1.547		1.575	0.028	0			4
Silicosulfate		Orthorhombic	1.638		1.640	0.002	60			2
Thaumasite		Hexagonal	1.470		1.504	0.034	0			2
			1.464–1.468		1.500–1.507	0.036–0.039				4
Tobermorite-11 Å		Orthorhombic	1.570 ± 0.002	1.571 ± 0.002	1.575 ± 0.002	0.005	+Small			1
Tricalcium aluminate	C_3A	Cubic		1.710		Isotropic				2,6
Tricalcium aluminate, Fe-bearing	C_3A	Cubic		1.735						2
Tricalcium aluminate, Na-bearing	NC_8A_3	Orthorhombic	1.702		1.710	0.008	<35			6
Tricalcium silicate hydrate	C_3SH_2		1.586–1.592		1.594–1.600	0.008			+	1
Vaterite		Hexagonal	1.650		1.550	0.010	+			4

References: 1 Heller and Taylor (1956) and references therein, 2 Taylor (1998) and references therein, 3 Tröger (1982), 4 Winchell (1951), 5 Carpenter *et al*. (1960), 6 St. John *et al*. (1998).

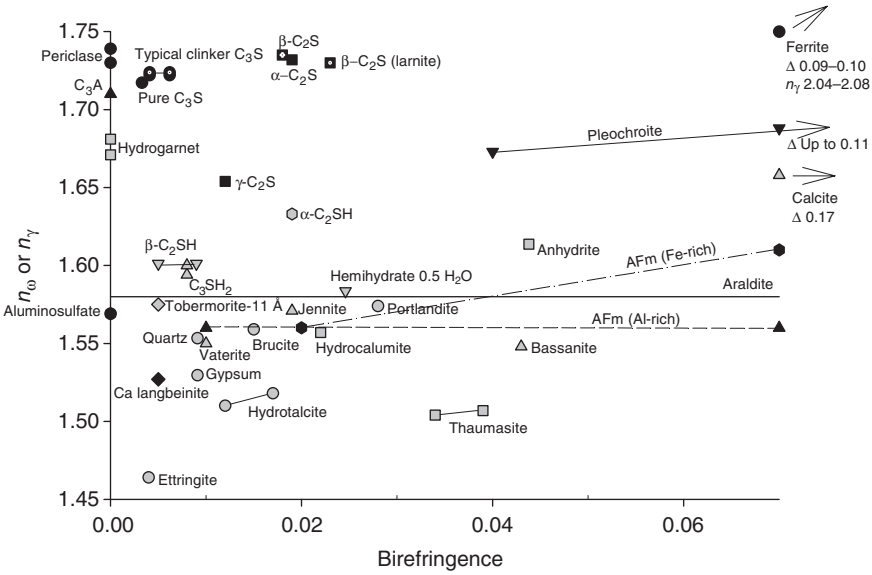

8.3 Determination table for hardened concrete, based on birefringence versus n_ω or n_γ being the largest refractive indices of optically uniaxial or biaxial phases, respectively. For comparision, quartz and the commonly used epoxy resin araldite are also indicated.

- Description of the concrete's characteristics on a mesoscale, such as aggregate distribution, voids, cracks, and delamination. This may be done without prior preparation of the cores, though prior vacuum impregnation with a UV-fluorescent resin may make it more easy to detect cracks. In the case of severely cracked concretes, analysis of flat-polished vacuum-impregnated slabs made from the cores, so-called fluorescence macroscopic analysis (FMA), may be appropriate. This method often may yield valuable information on crack distribution, depth and intensity (e.g. Polder and Larbi 1995).
- Thin section preparation (see section 8.3), including deciding from which part of a core or sample the thin section will be made.
- Investigation of a thin section of concrete using polarizing-and-fluorescence microscopy, PFM (see section 8.1). In many cases, microscopic investigation will be limited to PFM. Occasionally, however,
  - higher resolution at higher magnification may be required and PFM may be followed by scanning electron microscopy (SEM), either on the same polished (not-covered) thin section, or subsamples from the core-, or other microscopic techniques, or
  - optical phase identification is not unambiguous and phase identification may be supplemented by using energy dispersive spectrometry

(EDS) or wavelength dispersive spectrometry (WDS), using either a scanning electron microscope or electron microprobe analysis (EMPA), or by x-ray diffraction analysis (XRD). Potts *et al*. (1995) give a good introduction to microchemical analysis. It should be realized, however, that for cement-based materials, (sub)microscopic intergrowths are rather common, complicating identification of phases by microchemical analysis (Bonen and Diamond 1994).

- Evaluation of the results from the microscopical analysis in the light of macro- and mesoscale observations. An adequate diagnosis of concrete deterioration requires that this diagnosis is consistent with the observed features at all scale levels, that is microscopic, mesoscale (hand specimen) and macroscale (construction). For example, the occurrence of a single aggregate grain showing alkali–silica reaction (ASR) in a thin section does not necessarily demonstrate that damage of a construction is caused by ASR. On the other hand, the map cracking with white deposits does not demonstrate ASR, if no reacting aggregate is present.

Components in concrete, such as air voids or potentially alkali–silica reactive aggregate particles, may be quantified using *point counting*. Various standards, such as ASTM C457 (2008) outline standard procedures for quantitative determination of the various components and constituents in hardened concrete based on point counting. Reliability of point counting results was originally discussed by Van der Plas and Tobi (1965) and revised by Howarth (1998). Generally, an error of less than 2% may be obtained (French 1991). A similar method, invoked for the determination of fly ash (PFA) and slag (GGBS) contents, is the so-called *line method*, in which the number of non-hydrated fly ash or slag and clinker particles is point-counted and evaluated using standards (French 1991, Fox and Miller 2007). In interpreting such results, however, it should be realized that original binder constituents, such as fine-grained blast furnace slag, may have completely reacted, resulting in an underestimation of their original amount (Lindqvist *et al*. 2006). Cement contents may be calculated from point counting analysis by combining results with volume and real density of a cement paste (French 1991, Larbi and Heijnen 1997).

8.3 Sample preparation

Preparation of a thin section starts with selection of the part of the concrete that is to be examined. This is cut from the core or sample using a diamond saw. Typically, this piece of concrete will fit a thin-section glass of 30 mm × 50 mm, but larger thin sections up to, for example, 100 mm × 150 mm may also be used, especially if one wants to study any deleterious effects

with depth from the surface. If the concrete has disintegrated severely or shows severe cracking, the entire core may first be impregnated before cutting the subsample for the thin section. Powder samples may be mounted in resin and allowed to harden before using. The subsample is usually dried at about 40 °C, and vacuum-impregnated with an appropriate resin (e.g. araldite) to which a fluorescent dye is added.

Subsequently, the subsample may be glued to a supporting glass slide, though this is not essential. The side of the subsample that will be glued to the glass of the thin section is ground and finely polished. Sometimes, second impregnation and polishing is required. The next stage is to glue the thin section glass to the finely ground side, after which the remaining material is cut off using a thin diamond saw. The thin section is subsequently ground and polished down to a thickness of about 25 μm. Whereas geological thin sections commonly have a thickness 30 μm, thin sections for concrete petrography should be slightly thinner, that is, about 25 μm, in order to discriminate within the cement paste and the other components. For study of individual clinker phases, a thickness of about 20 μm is desirable in order to prevent overlap of crystals. Finally, the thin section is covered with a special cover glass to prevent it from being damaged in the course of time. Usually, a UV-hardening glue is used for the cover glass. However, if future examination of the same thin section using for example scanning electron microscopy or microanalytical techniques is expected, the cover glass should not be applied.

Any water used as a coolant in the preparation of thin sections, may affect the sample. This is particularly true for soluble salts such as halite, NaCl, which will be removed during the preparation process. Therefore, if the presence of soluble salts is suspected as part of the damage process, other coolants, such as glycol, may be considered. For non-hydrated binder samples such as clinker, oil may be considered to prevent sample alteration.

The intensity of fluorescence of fluorescent dyes may be reduced significantly when exposed to light for a long time. For this reason, thin sections prepared with resins containing fluorescent dyes should be stored properly.

8.4 Petrographic analysis

8.4.1 Sound concrete

Any petrographic investigation of concrete will try to resolve the nature of the original, undamaged concrete. One or more cores from a part of a structure not affected by damage processes may serve as reference. The following information should be obtained:

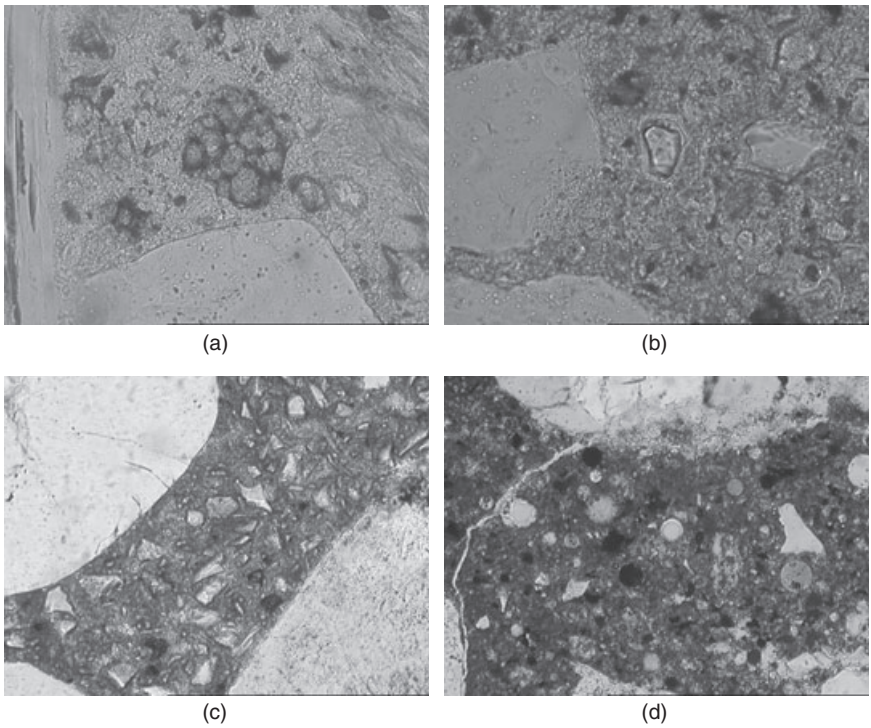

8.4 Microphotographs showing examples of: (a) Portland clinker constituent C_2S (belite); (b) Portland clinker constituent C_3S (alite); (c) ground granulated blast-furnace slag (GGBS); (d) pulverized fuel ash (PFA) (all microphotographs are taken in plane polarized light, view 0.35 mm × 0.22 mm, except (d) 0.7 mm × 0.45 mm).

- *Type of binder*. The presence and amount of non-hydrated binder (constituents, such as clinker phases (C_2S, C_3S, C_3A; Fig. 4a and b), ground granulated blast-furnace slag (GGBS; Fig. 8.4c) or pulverized fuel ash (PFA; Fig. 4d) may indicate the nature of the binder used. In most cases, however, it may not be possible to distinguish between prefabricated cements such as CEM II/B-V or CEM III/A and CEM III/B, and mixtures of CEM I and either PFA or GGBS, respectively. It should be realized that the nature of binder constituents may have changed over time. Early-20th-century blast-furnace slags used in concrete contain much larger and more crystalline phases than the glassy ones of today (Fig. 8.5); clinker itself was also more coarse grained. More fine-grained supplementary cementing materials, such as silica fume (SF) or trass may be difficult to identify, especially at old age, except when they exist as agglomerates.

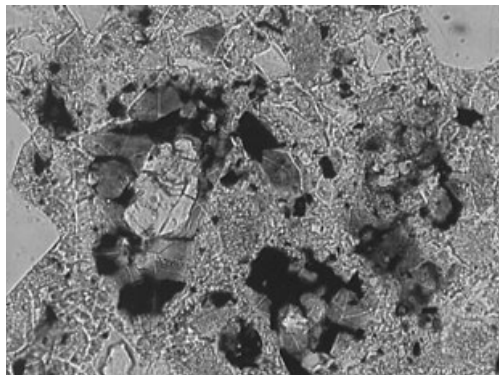

8.5 Microphotograph showing 1920s blast-furnace slag in concrete, containing relatively large crystalline phases (plane polarized light, view 0.35 mm × 0.22 mm).

- *Type, grading and distribution of the aggregate and fillers*. This aspect deals first with establishing the type of aggregate used and whether or not it is homogeneously distributed. Is there only aggregate, or have also inert fillers been used? Does the aggregate consist of well-rounded river or sea dredged sand and gravel, crushed rocks, or secondary or recycled materials, including concrete and masonry granulates. Are petrographic types of aggregate present that are prone to a specific damage process? Potentially deleterious constituents of aggregate include compounds that are alkali–silica (e.g. porous chert, chalcedony, opal, some impure limestones) or alkali–carbonate (e.g. dolomitic limestone) reactive, clay or organic matter, compounds containing soluble lead, zinc, cadmium, alkalis, chlorides or sulfates, absorptive and microporous grains. (Brown and Sims 1998).
- *Hydration of binder*. Degree of hydration may be assessed by evaluating the amount of non-hydrated binder components relative to the hydration products formed; the relative amount and distribution of portlandite (calcium hydroxide, CH), may also give an indication (Fig. 8.6). It is important to note that hydration will cause microcracking owing to chemical shrinkage and possibly the heat associated with hydration of the cement, especially in massive and heat-cured concretes. Experience shows that most concretes are microcracked to some extent. This should be taken into account when newly formed cracks are evaluated.
- *Aggregate–cement paste interface*. The interface between cement paste and aggregates is important in determining both its mechanical and durability properties. Debonding or lack of adhesion between cement paste and aggregate will be visible microscopically, as will primary hydration products, such as portlandite and ettringite, at the interface.

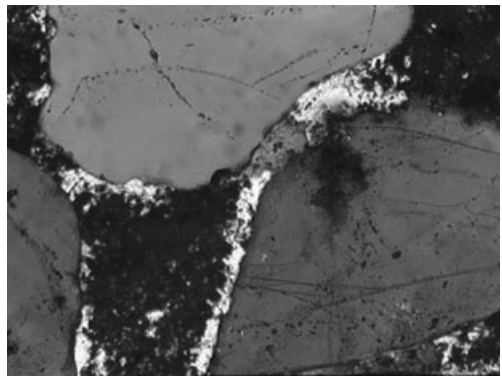

8.6 Microphotograph showing relatively coarse-grained portlandite crystals at the interface between cement paste and aggregate (cross-polarized light, view 0.7 mm × 0.45 mm).

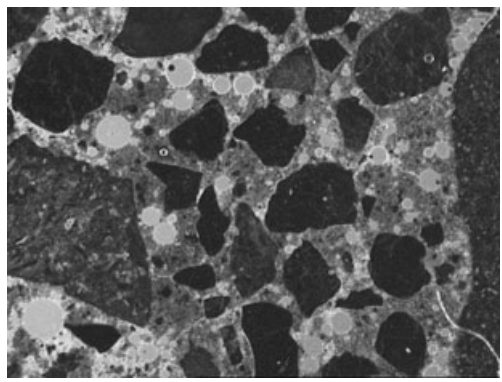

8.7 Microphotograph showing the abundant air voids induced by an air entraining agent under UV fluorescence (view 5.4 mm × 3.5 mm).

- *Air content, void shape and distribution*. The amount of entrapped air, the shape and distribution of air voids may demonstrate the use of air entraining agents (Fig. 8.7), undesired interaction between cements and, in some instances, plasticizers or (super)plasticizers (see section 8.4 Delamination and debonding of overlays).
- *Other components*. Are there any other components present, such as steel (Fig. 8.8), glass, carbon or polypropylene fibres?
- *Water–cement ratio (w/c)*. A direct relationship exists between the number of capillary pores in concrete and the water–cement ratio (w/c) is given in Table 8.2. However, in optical light microscopy, pores smaller than 1 μm, that is, the capillary pores, cannot easily be seen. Use of fluorescence microscopy may overcome this problem (Fig. 8.9). Owing

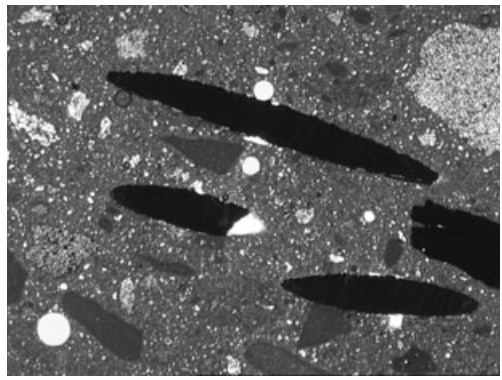

8.8 Microphotograph with example of steel fibres in high-strength concrete (plane polarized light, view 5.4 mm × 3.5 mm).

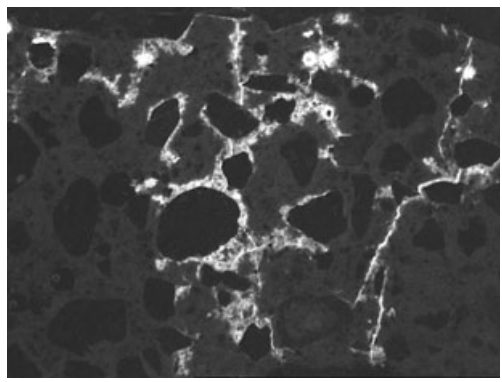

8.9 Typical UV-fluorescent microphotograph, illustrating higher w/c ratio along cracks and cement paste–aggregate interface (view 5.4 mm × 3.5 mm).

Table 8.2 Original water/cement ratio versus capillary porosity of cement paste (Christensen *et al*. 1979)

w/c (wt.%)	Capillary porosity (vol.%)
0.40	8
0.45	14
0.50	19
0.55	24
0.60	28
0.65	32
0.70	35
0.75	38
0.80	41

to vacuum impregnation of the specimen, a higher water–cement ratio will result in a higher amount of capillary pores, which, in turn, will absorb more resin, yielding a higher or brighter fluorescence. It should be realized, however, that the microstructure of concrete is not static. It changes with time. Capillary porosity changes with time (because of hydration of the cement and hydration or any reactive additions), and differs for different binders. Age and type of binder should be included in the microscopic determination of the w/c ratio, using appropriate reference standards. Microscopic determination of the w/c ratio is rather accurate. Usually, a reproducibility of 0.03 may be obtained (e.g. Jakobsen and Brown 2006), and may often reveal microscopic variations owing to segregation or microbleeding.

8.4.2 Evaluating concrete production

Future concrete deterioration of concrete structures may partially come from errors in concrete production, casting, pouring or placing, and compaction. For example, inadequate curing may result in the development of microcracks perpendicular to the concrete surface, owing to drying shrinkage. Mixing and segregation may be evaluated by searching for domains in the cement paste with less or no (fine) aggregates at a microscopic level, accompanied by assessment of the presence of cement or binder agglomeration, distribution of coarse aggregate at a mesoscale level. In fluorescence mode, effects of processes affecting capillary porosity, such as microbleeding, may be identified. Improper compaction may reveal local areas of poor bonding of cement paste to aggregate particles and excessive voids (Fig. 8.10).

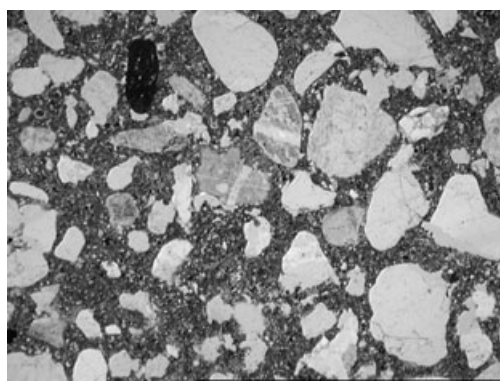

8.10 Microphotograph showing the effect of poor compaction of concrete (plane polarized light, view 5.4 mm × 3.5 mm).

8.4.3 Damage diagnosis

Microscopic diagnosis of damage involves the evaluation of any changes to the concrete microstructure or components present owing to ageing, loading or interaction with the environment to which it is exposed. In general, these changes may be:

- Excessive microcracking, scaling, spalling, delamination or pop-outs, owing to, among others, loading, frost differential expansions, or formation of new reaction products (Fig. 8.11).
- The presence of new phases, such as carbonate owing to carbonation or secondary ettringite, thaumasite, ASR gel or other deleterious reactions.
- Disappearance of phases originally present, owing to carbonation (conversion of portlandite to calcium carbonate), leaching or dissolution (partial or complete absence of portlandite) or thermal breakdown upon fire attack.

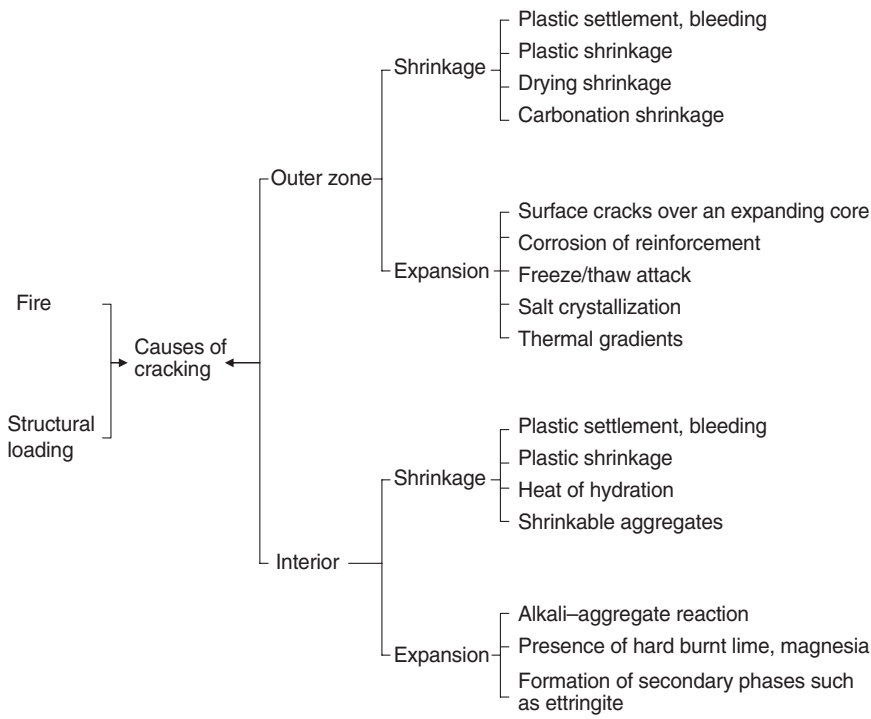

8.11 Schematic illustration of possible causes of cracking in concrete (modified after Sims and Brown 1998 and St. John *et al.* 1998).

- Changes in (capillary) porosity owing to precipitation, dissolution or thermal breakdown of phases, but also owing to continued hydration reaction of binder.

Carbonation

Carbonation is the chemical reaction between carbon dioxide (CO_2) from the atmosphere and the cement paste in concrete or mortar. Calcium hydroxide in the cement paste matrix is converted to calcium carbonate ($CaCO_3$); over a longer period, the calcium silicate hydrate (CSH) phase may also be carbonated. Carbonation of concrete will affect porosity and permeability of the concrete (and hence durability) or result in corrosion of embedded reinforcement. Corrosion of reinforcement steel is usually easily diagnosed without microscopic investigation. Carbonation of the cement paste is, however, easily detected in cross-polarized light (Fig. 8.12). Its effect on porosity may also be observed. For ordinary Portland cement concrete, for example, capillary porosity of the carbonated zone will be lowered relative to the original uncarbonated cement paste. In case of concrete made with ground granulated blast-furnace slag cement, porosity will be increased in the carbonated zone.

Leaching, dissolution

Leaching in concrete occurs when acid waters, usually containing atmospheric acid gases such as SO_2, NO_x and CO_2, interact with concrete, causing the acid-soluble constituents in concrete to dissolve and be transported to other sites where they recrystallize or precipitate to form new compounds (Hewlett 1998, Larbi and Visser 1999). In thin sections, dissolution of constituents in concrete is marked by an increase in its capillary porosity and, as a consequence, it is more vulnerable to other forms of attack such as frost, wetting and drying and further leaching. Dissolution and leaching can also lead to loss of cohesion and strength of the surface layer of concrete owing to volume changes, which may negatively affect the integrity of the concrete, especially if a coating is applied. In the latter instance, it may affect the bond and, in severe instances, cause spalling of the coating. When efflorescence occurs on concrete, it is usually related to an aesthetic form of deterioration, but efflorescence can also eventually lead to surface deterioration of concrete itself as a result of material loss owing to spalling or flaking.

Acid attack

Acid attack is the dissolution and leaching of acid-susceptible constituents, mainly calcium hydroxide, from the cement paste of hardened concrete.

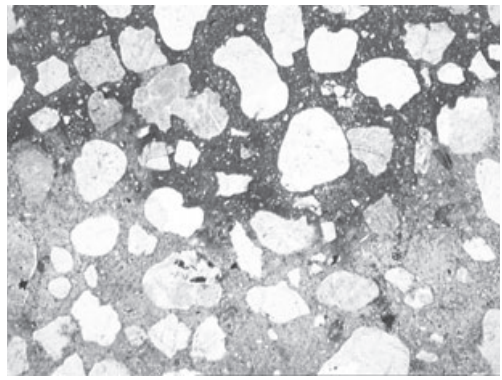

(a)

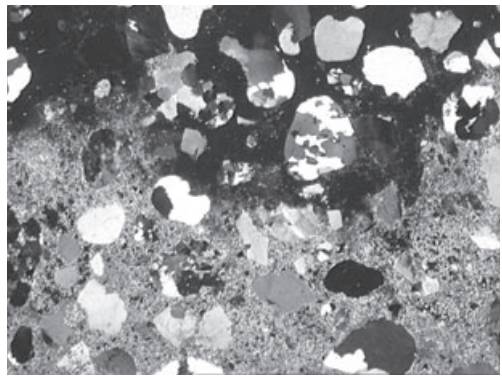

(b)

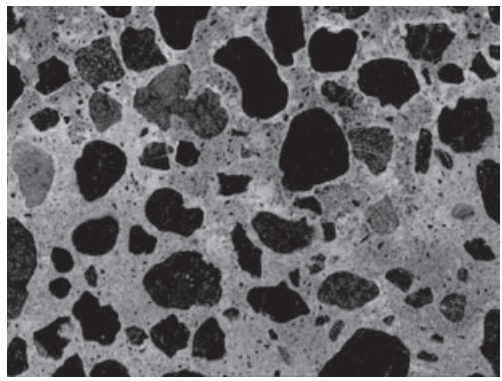

(c)

8.12 Microphotographs showing the effect of carbonation (lower part of images) on ground granulated blast-furnace slag concrete: (a) plane polarized light, (b) cross-polarized light, (c) under UV fluorescence (view 5.4 mm × 3.5 mm).

This action results in an increase in capillary porosity, loss of cohesiveness and eventually loss of strength. In pronounced instances, acid attack may be accompanied by crack formation and eventually disintegration, especially when the structure is subjected at one side to water pressure. Unlike sulfate attack (see below), the products formed from acid attack are not expansive, and leaching will only occur in structures that are relatively permeable. In high performance concrete systems containing cement pastes with a low content of calcium hydroxide, acid attack is relative slow and may involve only the finely divided calcium hydroxide crystals incorporated in the interstices of the calcium silicate hydrates, C-S-H.

The process is illustrated in Fig. 8.13. The micrographs obtained from PFM analysis, supplemented with SEM–EDS studies, reveal that only the top, surface portion of the concrete has been attacked by acidic solution. The rest of the concrete shows no form of deterioration. In the attacked zone, there is clear evidence of leaching of the cement paste matrix, leading to increased capillary porosity and loss of cohesion of the matrix. Locally, there is loss of bonding of the cement paste to aggregate, but on the whole, these aspects have not adversely affected the microstructure and quality of the concrete (Fig. 8.13). In this instance, long-term durability of the concrete is not likely to be compromised.

Alkali–aggregate reactions (ASR, ACR)

Alkali–aggregate reactions are reactions between reactive constituents in the aggregate with alkali hydroxides in the pore solution in the cement paste. In case of alkali–silica reaction (ASR), reactive aggregate contain relatively soluble, non- or poorly crystalline silica, combining with the alkali hydroxides to give a hygroscopic gel (Hobbs 1988). This gel may cause swelling and cracking of the concrete. Examples of such aggregates include opal, chalcedony, porous chert, some impure sandstones or greywackes, among others.

Alkali–carbonate reaction (ACR) is the chemical reaction between certain fine-grained, argillaceous dolomitic limestone aggregates in concrete and the alkali hydroxides in the pore solution of the cement paste. In the case of ACR, no gel is formed, but nevertheless swelling and cracking of the concrete might occur (Swenson 1957). It must be pointed out that the reaction of carbonate aggregates that produce only dedolomitization rims without deleterious expansion is not called ACR. Recent studies by means of SEM and EPMA, however, has revealed that, in some cases, cryptocrystalline quartz and ASR gel are present in the typical ACR aggregate in both field and laboratory concretes. In such cases, ASR may also be associated with ACR because ASR gel is often found in open spaces created by dedolomitization (Katayama 2004).

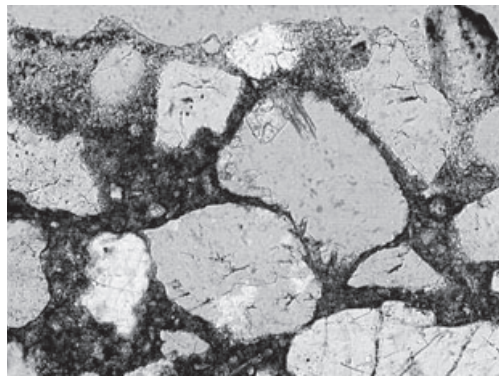

(a)

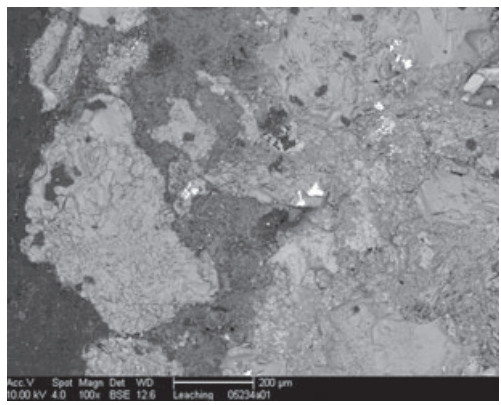

(b)

8.13 Acid attack of concrete: (a) micrograph showing the attacked zone along the surface of the concrete (plane polarized light, view 1.4 mm × 0.9 mm), (b) SEM–BSE micrograph of the same top portion of the concrete in the thin section. The leached zone appears dark-grey in this back-scattered SEM image, whereas further down, the concrete is not attacked and appears light-grey in colour.

In general, deterioration to concrete caused by AAR may be manifested at the external surface in several forms, which may include:

- Cracking, often in the pattern of 'map-cracking' (Fig. 8.14), occasionally filled with the reaction products (ASR gels in the case of ASR as exudations); the cracking pattern may also be longitudinally oriented in the direction of compression stresses (for example in reinforced or pre-stressed concrete units).
- Expansion, causing relative movements, displacements and deformations.

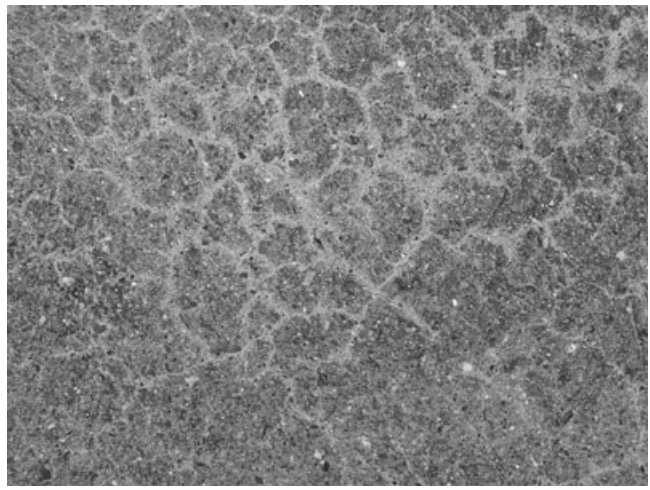

8.14 Typical macroscale map cracking owing to ASR.

- Surface discoloration, particularly along cracks.
- Scaling or spalling of portions of the surface.
- Surface pop-outs, often caused by reaction of coarse aggregate particles close to the surface.
- Debonding of composite layers.

Microscopically, AAR is manifested by microcracking with fine cracks propagating from reacting particles into the surrounding cement paste. Such incipient cracks are not evident in the visual inspection of field concrete. Within a structure made with the same concrete mix, the rate of cracking may vary, depending on the availability of water. With progressive AAR, expansion cracks propagate, interconnecting the reacting particles in a random network, some of which widen towards the concrete surface. Usually, the cracks skirt inert aggregate particles. At a macroscopic level, the late stages of AAR, in which expansion of concrete has almost ceased and cracks have become old, damage has become most conspicuous, including the maximum development of crack widths, exudations and any displacements. In such concrete, both cement paste and ASR gel near the cracks are likely to be more or less carbonated, and precipitation of calcium carbonate or calcite into open spaces can be seen.

Recognition of ASR around 1940 (Stanton 1940) prompted detailed petrographic characterization of aggregates for use in concrete. Currently, assessment of the amount of potentially alkali–silica reactive components in the aggregate is part of guidelines for the prevention of deleterious ASR in concrete (e.g. RILEM TC 191-ARP, 2003, CUR Recommendation 89).

8.15 Microphotograph showing cracks filled with ASR gel along porous chert (plane polarized light, view 5.4 mm × 3.5 mm).

A concise overview of (potentially) alkali–aggregate reactive aggregate types is given by Lorenzi *et al*. (2006).

Diagnosis of ASR as cause of damage is, however, often complicated by the fact that, in many cases, ASR is accompanied by the formation of massive secondary ettringite, making the question of the (main) cause of damage ambiguous (e.g. Shayan and Quick 1991, Thomas *et al*. 2008). Clear petrographic evidence of the following features may demonstrate the occurrence of ASR:

- Cracking through aggregate grains and cement paste.
- Involvement of (potentially) alkali–silica reactive aggregate constituents (Fig. 8.15), that is, aggregate particles containing relatively easy alkali-soluble silica, such as porous chert, chalcedony, opal, some impure sandstones, and some limestones containing biogenic silica.
- Presence of ASR gel in cracks (Fig. 8.15). Especially if the reactivity of aggregate is relatively high (aggregates containing opal, chalcedony, cristobalite and hydrated rhyolitic glass), cracks may be filled with abundant ASR gel, and the soaking of ASR gel often darkens the bordering cement paste.
- Extrusion of ASR gel from reacted aggregate into adjoining cement paste (Fig. 8.16).
- Presence of ASR gel in air voids (Fig. 8.17).
- Partial internal dissolution of aggregate particles.

A combination of these features forms the complete body of evidence for deleterious ASR. The first four features are most important. Partial internal dissolution of aggregate particles is only occasionally encountered in samples retrieved from concrete structures, but common in laboratory specimens from other test methods such as the ultra-accelerated mortar bar

8.16 Microphotograph showing extrusion of ASR gel from impure sandstone into the adjoining cement paste (plane polarized light, view 2.8 mm × 1.8 mm).

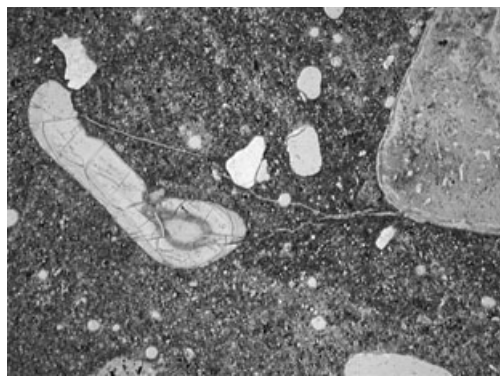

8.17 Microphotograph showing void filled with ASR gel (plane polarized light, view 5.4 mm × 3.5 mm).

test (RILEM TC 106-2, 2000) (Fig. 8.18). The presence of some ASR gel in voids alone, which is not associated with cracking through aggregate and cement paste, may indicate (initial) ASR, but does not necessarily demonstrate deleterious ASR. Evaluation of the amount of aggregate particles involved, the total amount of ASR gel, and the intensity of (micro)cracking may give an indication of the extent of ASR. Results of the microscopic investigation should be considered in the context of a full structural evaluation of a structure, as outlined in Dutch CUR Recommendation 102 (2008), for example.

There is no special method or procedure for diagnosing damage of concrete owing to ACR. Petrographically, an approach similar to that for ASR

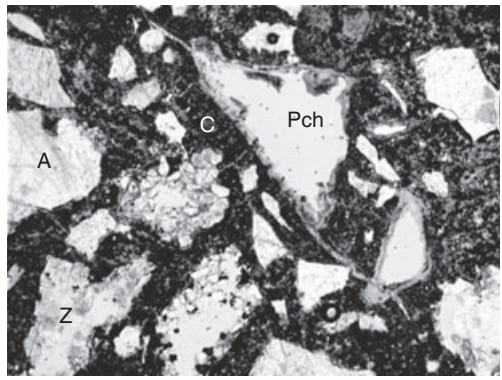

8.18 Microphotograph showing almost completely dissolved alkali–silica reactive aggregate grains after 14-day ultra-accelerated mortar bar test (plane polarized light, view 5.4 mm × 3.5 mm). A, aggregate; C, cement paste; Pch, porous chert; Z, sandstone.

may be followed. The major difference is that, for ACR, it has to be established whether dolomitic aggregates are present and dedolomitization or breakdown of dolomite rhombs has occurred. Unlike ASR, no gel is formed. If dedolomitization has occurred, it is essential to establish whether this is the primary cause of damage. At an advanced stage of ACR, relatively large, well-developed brucite crystals may be observed around reacted aggregate particles.

Sulfate attack

Sulfate attack is the reaction between sulfate ions in the pore solution of concrete and constituents in the concrete that result in formation of new reaction products with a relatively large molar volume. If sufficient new phases are formed, stresses can be induced in the concrete to such an extent that the concrete can undergo cracking. The sulfate ions may either come from the concrete itself, that is, when the sulfate content of the cement is excessively high or from external sources, when the environment in which the concrete is placed is rich in sulfates.

There are two main forms of sulfate attack, each yielding an expansive product, but with different compounds. The first and most common form of sulfate attack involves reaction of sulfate ions with calcium hydroxide and tricalcium aluminate hydrates in the cement paste leading to the formation of gypsum ($CaSO_4.2H_2O$) and massive ettringite, ($3CaO.Al_2O_3.3CaSO_4.32H_2O$ or $Ca_6Al_2(OH)_{12}(SO_4)_3.26H_2O$) (Fig. 8.19). The reaction occurs at normal temperatures under relatively moist conditions. Because the reaction begins with dissolution of calcium hydroxide from the

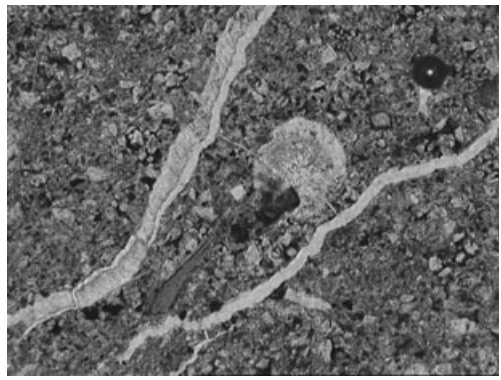

8.19 Microphotograph showing cracks and air voids filled with massive secondary ettringite (plane polarized light, view 5.4 mm × 3.5 mm).

cement paste, a typical effect is an increase in the capillary porosity of the cement paste. The second form of sulfate attack in concrete and other cement-based composites leads to the formation of thaumasite ($CaSiO_3$.$CaCO_3$.$CaSO_4$.$15H_2O$ or $Ca_3Si(OH)_6(CO_3)(SO_4).12H_2O$). It is similar to ettringite in its formation, however, unlike ettringite in which tricalcium aluminate hydrates are involved, it is the calcium silicate hydrates (the C-S-H, i.e. the main strength-giving component) within the cement paste that are affected.

In general, structures affected by sulfate attack usually exhibit large deformations caused by swelling leading to crack formation. At the construction level, the cracks often form a polygonal network and very often contain colourless or white exudations. In the laboratory, diagnosis of cores removed from structures affected by sulfate attack begins with a visual inspection, using a hand lens or a stereomicroscope. The pattern of cracking, especially along the surface of the aggregate particles can provide clues as to the cause of deterioration. For massive ettringite or thaumasite formation, large, dense amounts of the ettringite or thaumasite crystals are produced, causing some to precipitate as white exudations in most of the voids at the surface of the cores and on the fractured or sawn surfaces. Small amounts of these fillings can be scraped onto glass plates, dispersed in immersion oil and examined with the aid of a transmitted light microscope. If deterioration is caused by massive ettringite (Fig. 8.19) or thaumasite formation, dense almost indistinguishable needle-like crystals, together with calcium carbonate crystals and some fine sand or cement particles shall be detected. This preliminary diagnosis gives an indication that the deterioration is most likely caused by massive ettringite or thaumasite formation. Since the visual deterioration features of sulfate attack are similar to other

forms of attack, for instance, frost attack accompanied by leaching of the cement paste, further diagnosis either by means of PFM or SEM–EDS is required. Both techniques are equally suitable, but the PFM technique is more suitable because larger thin sections with surface area of about 100 mm × 150 mm can be investigated than in the case of SEM.

Massive secondary ettringite (delayed ettringite formation, DEF)

Ettringite is a primary constituent of hydration of Portland cement concrete. Its formation plays an important role in the control of setting. Minor amounts of secondary ettringite are often encountered in air voids of hardened concretes, regardless of the type of cement used. This secondary ettringite, evidently developed in the walls of the air void, become stable, but is not associated with any cracking. Individual ettringite crystals are easily distinguished. Less commonly, massive secondary ettringite is encountered. Microscopically, this ettringite takes the form of massive aggregates or bands at the aggregate–cement paste interface, causing debonding, or filling cracks, accompanied by air voids (almost) completely filled by ettringite (Fig. 8.19). The majority of the individual ettringite crystals in the aggregates cannot be distinguished. Cracking may be intense, and, sometimes, massive secondary ettringite occurs together with ASR (see previous subsection).

Massive secondary ettringite is often denominated as delayed ettringite formation, DEF. Originally, this term was reserved for secondary ettringite formed in concretes that are heat or steam cured above 70 °C (Taylor *et al.* 2001). Above this temperature, primary ettringite is destabilized. Subsequently, massive secondary ettringite forms, in which individual needle-like crystals cannot easily be distinguished with the aid of an ordinary optical microscope. DEF may cause swelling of the hardened concrete, increase microcracking, increase the capillary porosity, reduce the cohesiveness of the cement paste and cause debonding of the cement paste from the aggregate particles. DEF should not be confused with secondary ettringite, which forms in cracks or air voids in concrete by solution and re-precipitation of primary ettringite. This secondary ettringite reaction may occur in concretes cured at normal temperatures.

Massive secondary ettringite may also be the result of other causes, either by infiltration of sulfate from external sources like soils, groundwater, or materials stored in or at the surface of the concrete (such as fertilizer or artificial manure), or an excess of sulfate in the concrete itself, especially in historic concretes. Modern ground granulated blast-furnace slag cements (CEM III/A, CEM III/B) show a good resistance to sulfate attack. In the past, however, in similar cements (i.e. with similar slag contents, not supersulfated cements) calcium sulfate was not added to control setting, but in

much higher amounts, as it was considered needed to activate the slag (Van der Kloes 1924). This surplus of initial sulfate may be a cause of future massive secondary ettringite.

Thaumasite sulfate attack

The thaumasite form of sulfate attack on concrete is potentially more dangerous to concrete than massive secondary ettringite formation. This is because, in contrast to the latter, C-S-H phases are consumed, eventually resulting in complete disintegration of the cement matrix. Necessary conditions for thaumasite formation are (Hartshorn and Sims 1998, Sibbick *et al*. 2003):

- sufficient calcium silicate, sulfate and carbonate ions; the latter do not necessarily have to come from an internal source such as limestone aggregate or filler,
- initial reactive alumina, 0.4–1 wt.% of aluminium,
- high relative humidity or excess water, that is a consistently moist environment,
- low temperature, often <15 °C, but preferably 0–5 °C.

Thaumasite formation typically proceeds from the outside into the interior of concretes, with a four-stage zoning (Sibbick *et al*. 2003):

- *Zone 1* – No visual damage, but some microscopic presence of thaumasite and/or ettringite in air voids or at the cement paste – aggregate interfaces.
- *Zone 2* – Thin cracks lined with thaumasite ± occasional calcium carbonate parallel to the concrete's surface.
- *Zone 3* – Abundant, wider subparallel cracks, lined with thaumasite and occasional precipitated calcium carbonate; haloes of thaumasite around aggregate particles. Limited portlandite is present in the cement paste in both zones 2 and 3.
- *Zone 4* – Complete disintegration of the cement matrix owing to its replacement by thaumasite.

The reaction front between concrete affected by thaumasite formation and sound concrete may be very sharp. Another typical form of thaumasite development, not developing from the outside to the interior, is its formation at the interface between different cement-based materials, such as concrete or mortar and injection grouts (Fig. 8.20).

Both ettringite and thaumasite form needle-shaped crystals, though individual crystals may be difficult to identify in dense masses of crystals. In particular, in the early stages of deterioration, it will be difficult to discriminate between sparse, small crystals of thaumasite and ettringite. Typical features to distinguish thaumasite formation from that of secondary ettrin-

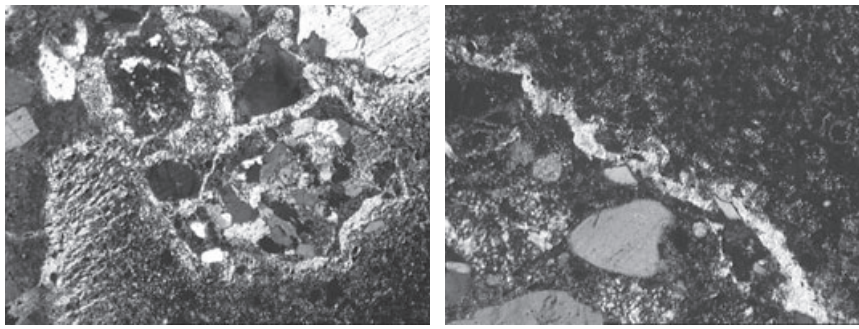

8.20 Thaumasite form of sulfate attack: (a) microphotograph showing formation of thaumasite around aggregate grains and within cement paste of mortar (cross-polarized light, view 2.8 mm × 1.8 mm); (b) microphotograph showing formation of massive thaumasite at interface between shrinkage-compensating injection grout and mortar in the same thin section (cross-polarized light, view 1.4 mm × 0.9 mm).

gite are the formation of crystals not only in air voids, in cracks or at the cement paste–aggregate interface, but also in the cement matrix itself. In addition, thaumasite has a higher birefringence, but the latter may be variable, possibly depending on its carbonate content, with low birefringent crystals of thaumasite also occurring (Sibbick *et al*. 2003).

The sulfate attack leading to the formation of thaumasite does not only lead to an increase in the capillary porosity of the cement paste or binder, but tends to soften the hardened cement paste, which, in turn, causes loss of cohesion and eventual disintegration of the concrete. Fig. 8.20 shows thaumasite developed owing to interaction between a shrinkage-compensating grout and masonry mortar. Such formation of thaumasite is accompanied by an increase in capillary porosity associated with the reaction.

Freeze–thaw damage

Deterioration of concrete as a result of frost occurs when concrete is subjected to alternating freezing and thawing. Deterioration is initiated by water absorbed in the capillary pores or entrapped in cavities of the concrete. In the absence of de-icing chemicals, freezing starts to occur when the temperature drops below –2 °C and thawing occurs when the temperature rises above 0 °C. The freezing process causes the water to increase in volume up to about 9%, leading to the development of large stresses that may exceed the strain tolerance of concrete. Repeated cycles of freezing and thawing may cause the hardened concrete material to develop cracks,

(a)

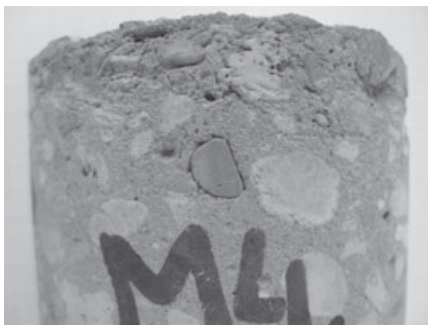

(b)

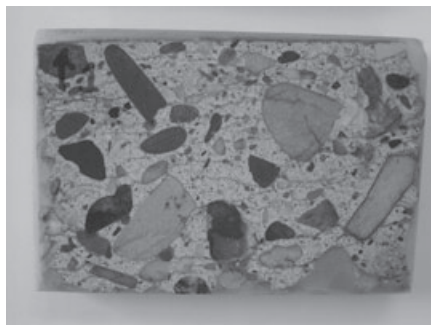

(c)

8.21 Freeze–thaw damage of concrete at macro-, meso- and microscales: (a) scaling of concrete of a railway bridge owing to freeze–thaw attack; (b) core of frost damaged concrete; and (c) an impregnated slab revealing cracks owing to frost, even through some aggregate particles.

followed by flaking, scaling and spalling at the surface (Fig. 8.21). These effects may gradually extend deeper into the concrete causing strength loss, debonding of cement paste from aggregates, loss of cohesion and ultimately total disintegration. The effects of frost are more pronounced in concrete in parts of the structure that become frozen whilst continuously wet for a long period of time. As with other forms of attack, such as leaching, the susceptibility of hardened concrete involved in the deterioration process depends on its internal pore structure in particular, the presence and intensity of intrinsic defects such as cracking, bursting and flaws and inhomogeneities arising from improper production processes.

Microscopically, the effects of deterioration because of frost in the concrete are manifested by microcracking, often along binder–aggregate interfaces, but also through porous aggregate particles and often parallel to the exposed surface, loss of the binder–aggregate bond, loss of cohesion of

cement paste or binder, local surface scaling and, in severe cases, spalling (Fig. 8.21).

Fire damage

Heating of concrete, by fire or otherwise, will result in a variety of structural changes like cracking, spalling, debonding of aggregate and rebars, expansion and loss of strength of reinforcement steel, expansion and mineralogical/chemical changes of the hardened cement paste such as discoloration, dehydration, dissociation, depending on the length of exposure to the fire and the maximum temperature attained. In the cement paste, evaporation and dissolution, dehydration and dissociation of ettringite, gypsum, calcium hydroxide, calcium carbonate and other phases such as the calcium silicate hydrates may occur (St. John *et al*. 1998). A combined meso- and microscale approach may use these reactions, as well as those in the aggregate, to trace the temperature distribution in concrete (Larbi and Nijland 2001, Nijland and Larbi 2001), which may be relevant in assessing structural safety, but also in forensics.

A combination of visual examination, using a stereomicroscope, and polarizing microscopy, may reveal several isotherms in the concrete (Fig. 8.22). The (dis)appearance of phases in the cement paste can be used to

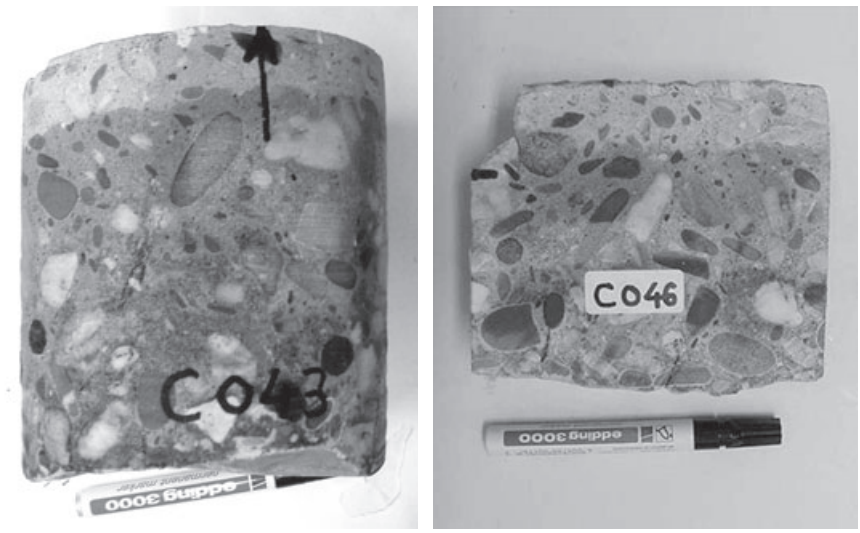

(a) (b)

8.22 Colour zoning in concrete made with blast-furnace slag cement (CEM III/B), owing to fire. Cores (a) and (b) show zoning from normal greenish blue to reddish beige (especially aggregate grains show iron oxidation) to whitish grey near the surface.

define additional isograds as a function of depth from the surface of the concrete. In addition to the concrete itself, remnants of burnt materials collected from the structure can offer additional information for estimating the maximum fire temperature reached. All these are summarized in Table 8.3.

Detailed information regarding the distribution of cracks, including fine microcracks (cracks with widths usually less than 10 μm) and the integrity (preservation of the compactness) of the concrete with depth from the fire-exposed surface may be obtained using flat-polished fluorescent sections. Such sections can be prepared from drilled cores and examined under UV light. Information on the density and the distribution of microcracks is useful in determining the thickness of concrete (from the spalled surface) that eventually needs to be removed in the case of repair work. It is also important in determining whether fire-attacked elements and components (including reinforcement steel) are still structurally sound and that the local loading conditions, in the long-term would not adversely affect the mechanical properties and the durability of the elements. Examples of polished slabs showing cracking as a result of heating are shown in Fig. 8.23.

Other forms of deterioration

Other forms of concrete deterioration may include pop-outs, debonding of coatings and delamination of top-surface layers of screeds in large concrete floors.

Pop-outs

Pop-outs in hardened concrete surfaces, such as floors, ceilings or walls are deformations, usually fracture, developed from particles or constituents lying just below the surface. They consist of two parts: a crater-like pit and the detached portion, which is spalled from the concrete (Fig. 8.24). The detached portion is usually cone-like and very often contains remnants of the particle or material responsible for the pop-out (Larbi and Visser 1999).

Pop-outs may vary in size from less than 10 mm to more than 100 mm in diameter at the surface and vary up to 40 mm in depth, depending on the particle type, size, depth of concrete cover and other conditions. They may be caused by various actions, including particles of periclase, MgO present in aggregate and even alkali–silica reaction (ASR). Pop-outs can develop at the surface of floors, ceilings or walls when iron sulfides, such as pyrite, FeS_2, occur as contaminants in the aggregate oxidizes to iron sulfate, $Fe_2(SO_4)_3{\cdot}nH_2O$ (Larbi and Visser 1999). If this oxidation reaction occurs over the sulfide constituent, the volume increase associated with the reaction is so great that excessive expansion occurs. Because the reaction occurs

Table 8.3 Summary of isograds in fire-damaged concrete structures

	Concrete		
Temp. (°C)	Macroscopic	Microscopic	Other (fire debris) materials in structure
70–80		Dissociation of ettringite, causing total depletion of ettringite in the cement paste	
105	Normal, no apparent macroscopic changes in concrete; colour remains grey	Loss of physically bound water in aggregate and cement paste; this effect causes an increase in the capillary porosity and microcracking of the cement paste which can easily be recognized by fluorescent microscopy	
120–163		Dissociation of gypsum, causing its depletion in the cement paste	
250			Charring of timber
<300			
300–350	Oxidation of iron hydroxides like FeO(OH) in aggregate and cement paste to hematite, α-Fe_2O_3, causing a permanent change of colour of the concrete from grey to pinkish brown		
450–500		Dissociation of portlandite, causing its depletion in the cement paste	

Table 8.3 Continued

Temp. (°C)	Concrete		Other (fire debris) materials in structure
	Macroscopic	Microscopic	
573	Transition of α-quartz to β-quartz, accompanied by an instantaneous increase in volume of quartz of about 5%, resulting in a radial cracking pattern around the quartz grains in the aggregate; this phase transition itself is reversible, but the radial cracking provides a diagnostic feature that remains after cooling		
600–800		Dissociation of carbonates; depending on the content of carbonates of the concrete; e.g. if the aggregate used is calcareous, this may cause a considerable contraction of the concrete due to release of CO_2; the volume contraction will cause severe microcracking in the cement paste	
650			Melting of aluminium alloys
>800	Complete disintegration of calcareous constituents of the aggregate and cement paste owing to both dissociation and extreme thermal stresses, causing a whitish grey coloration of the concrete	Final dissociation of calcium silicate hydrates, C-S-H and remaining phases in the cement paste resulting in complete disintegration of the concrete, with severe microcracking	
850			Melting of glass
1080			Melting of copper pipes

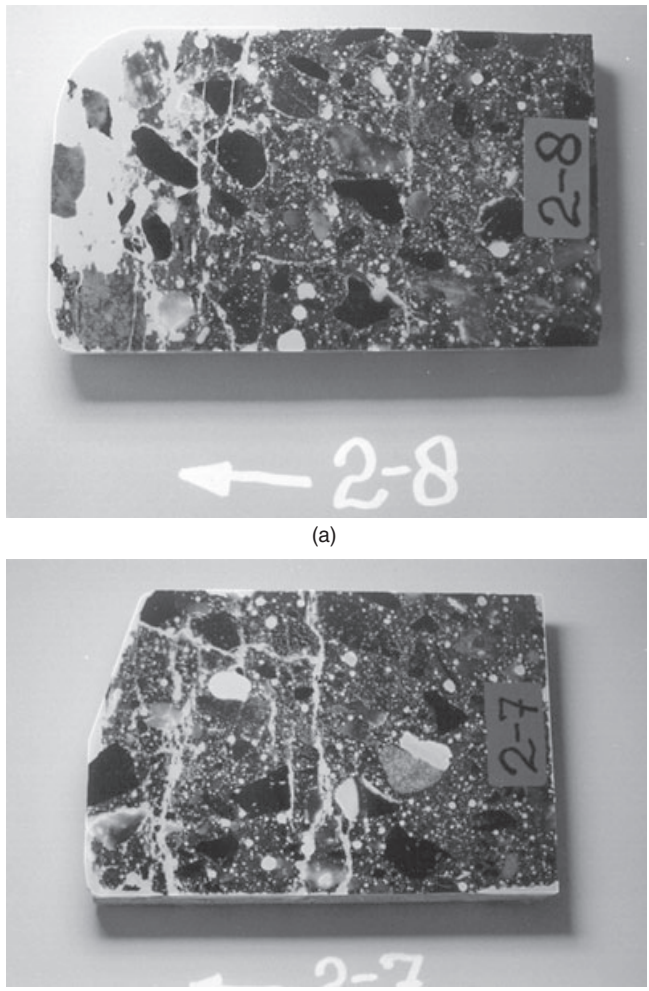

8.23 FMA macrographs (a) and (b) show the distribution of cracks in the polished sections prepared from cores removed from reinforced concrete linings of tunnel elements subjected to fire testing.

near the surface of the concrete, the stresses and strains developed in the surrounding cement paste are not balanced and pop-outs result.

At the construction level, diagnosis of the cause of pop-outs begins with visual inspection of the 'core' of the crater-like pit left behind after spalling and the surface of the cone-like portion (Fig. 8.24). In the laboratory, the visual inspection is extended further to the cone-like portions. This analysis can be supported with a stereomicroscope. In almost all instances, the particle or contaminant that is responsible for the formation of the pop-out

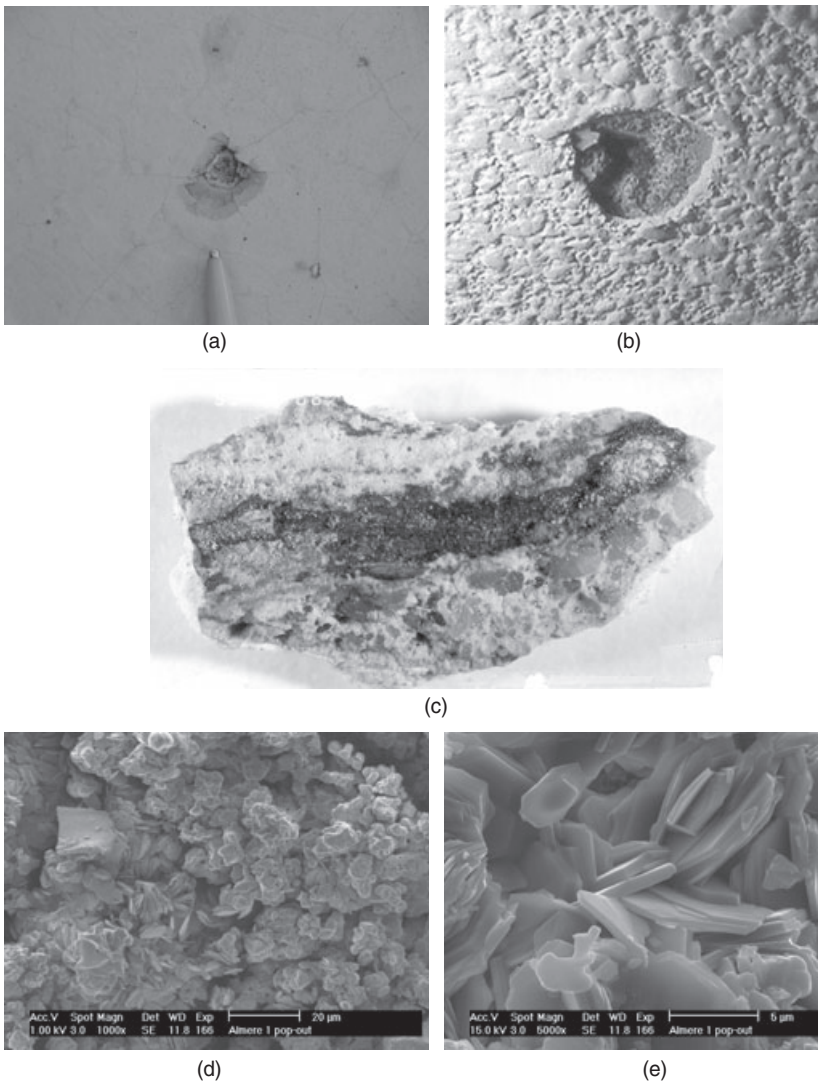

8.24 Pop-outs in concrete at macro-, meso- and microscale level: (a) and (b) show pop-outs on concrete floor and ceiling, with crater-like pits and remnants of the materials responsible for the pop-outs in the core of the pits; (c) a spalled pop-out from a concrete ceiling; (d) and (e) SEM micrographs showing (d) an overview and (e) detail of hydrated ferric sulfate responsible for pop-outs.

is found at the top of the cone or in the 'core' or centre of the crater-like hole left behind in the structure. For unstable iron sulfide contaminants, the reddish-brown colour produced by the oxidation process can be used to provide an indication of the reaction. If, however, the typical reddish-brown colour is absent, the analysis becomes complicated in which case

other techniques have to be employed. The type of unstable iron sulfide responsible for the pop-out, can be determined or verified by means of chemical analysis, but a quicker method is by means of a combination of SEM and EDS (Fig. 8.24). Pop-outs in the surface of concrete structures, in principle do not have any negative effects on the integrity of the structure. Rather they have only an aesthetic effect.

Delamination and debonding of overlays

Delamination is a separation along a plane parallel to a surface, as in the separation of a coating from a substrate or the layers of a coating from each other or, in the case of a concrete slab, a horizontal splitting, cracking, or separation near the upper surface. Delamination occurs frequently in bridge decks, floors and coatings and is caused by factors such as the corrosion of reinforcement steel, freezing and thawing and excessive shrinkage as a result of moisture loss. It is similar to spalling, scaling or peeling, except that delamination affects large areas and can often only be detected by tapping.

In some cases, additives may have undesired side effects. Though additives such as (super)plasticizers are not visible by optical or electron microscopy, some of these effects may be clearly discerned. Delamination of top-surface layers of large, monolithic concrete floors may be related to a significant increase in entrapped air, accumulating below the concrete's surface (Fig. 8.25). Evaluation of microscopic observations in combination with mix design shows that this is the result of interaction of a specific

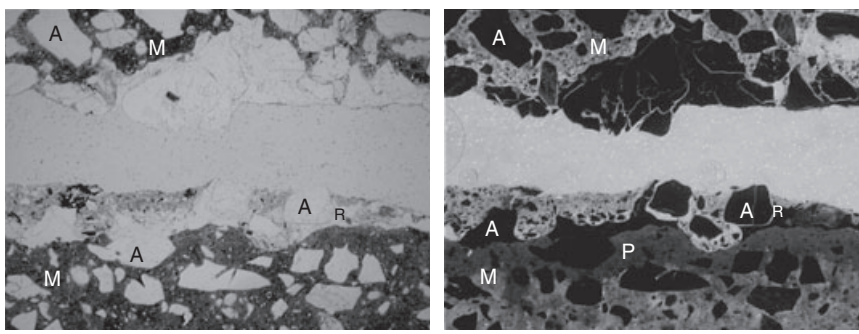

(a) (b)

8.25 Micrographs showing the debonded surface of a screed system showing the structure of the fracture surface and its vicinity: (a) in plane polarized light, the applied primer is not visible; (b) a UV fluorescent micrograph showing the revealed primer. Material in the top part of (a) and (b) is the screed (A, aggregate; R, hardened resin; M, matrix; P, penetrated resin or primer; view 2.8 mm × 1.8 mm).

superplasticizer with blast-furnace slag cement (STUTECH and STUFIB 2006).

Debonding of overlays is the physical separation along an irregular plane of a cement-based concrete, mortar or synthetic layer from an underground substrate. It often occurs when cement-based screeds are placed on concrete substrates which, before the placement may or may not have been treated with a primer. The porous nature of the substrate, the treated rough surface and the applied polymer-based primer, together with dry sand particles that are applied to the substrate's surface, ensure that sound bonding is achieved. After hardening, the sand particles, which protrude from the primer, serve as anchoring points for the screed layer. This system, in combination with the glue of cement paste fortifies the bond between the two layers. However, if poor or incompatible materials are used or the application is improperly carried out, bonding may not be optimum and separation of the screed may occur as a result of drying or thermal shrinkage (Fig. 8.25). A good bond is essential to resist shear forces in the bond plane caused by differences in drying and thermal shrinkage between the two layers.

Efflorescence

Efflorescence is just a deposit of salts, usually whitish in colour, formed on the surface of concrete. It is derived from compounds dissolved within the concrete, transported to the surface and deposited upon evaporation. When precipitation occurs directly on the surface, it is termed efflorescence. When dry, efflorescence usually appears as a white coating on the external surface of a concrete wall. A typical efflorescence is formed by calcium carbonate ($CaCO_3$). In more rare cases efflorescence of other salts, such as gypsum derived from carbon dioxide induced destabilization of ettringite, may occur (Brocken and Nijland 2004). Precipitation of leached products can also occur directly beneath the surface of concrete. In such a case, the deterioration mechanism is referred to as cryptoflorescence.

8.5 Evaluation of repairs

Concrete petrography may also be used to evaluate rehabilitation strategies, repairs and repair methods, by assessing the depth at which sound concrete starts. Figure 8.26 illustrates a case where a polymeric repair mortar was applied on fire-damaged concrete that was not brought back to the non-cracked substrate. It may also be used to assess the adhesion between different layers and materials (Fig. 8.27), such as repair mortars, gunnite or coatings. Microscopic investigation may also be used to assess the long term effect of electrochemical methods such as cathodic protec-

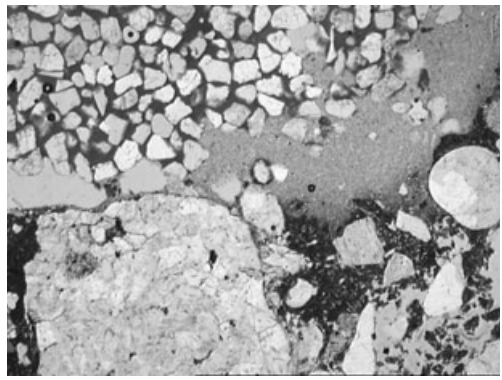

8.26 Microphotograph showing a polymeric repair mortar applied on fire-damaged concrete, that was not brought back to the non-cracked substrate (plane polarized light, view 5.4 mm × 3.5 mm).

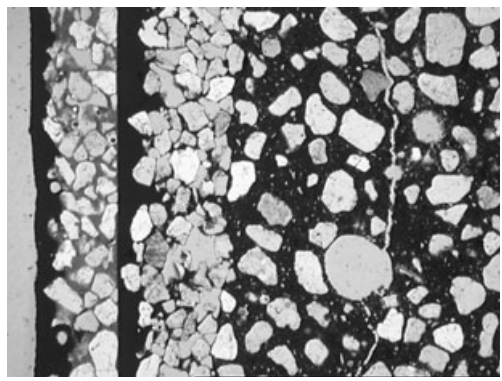

8.27 Microphotograph with example of successive surface finishes on concrete and surface parallel cracking in the underlying concrete (plane polarized light, view 5.4 mm × 3.5 mm).

tion. The long-term effect of inevitable acid production at the anode may be visible in an increase of capillary porosity of the cement paste around the anode (Polder *et al*. 2002).

8.6 Conclusions

Microscopy offers a quick and efficient method both for determining composition of (historic) concretes and for diagnosing the causes and extent of deterioration of concrete in structures. It also assists in providing both overview and insight into the mechanisms underlying various chemical forms of deterioration in concrete. Diverse forms of attack such

as alkali–aggregate reactions, sulfate attack, dissolution and leaching, frost and fire attack, which can adversely affect the internal structure of concrete, but cannot be seen with the naked eye, can be revealed with the aid of microscopy. Another useful aspect of microscopy is that it can be used to detect the occurrence of more than one form of deterioration mechanism present at the same time in concrete. In particular, it can be used to determine which of the mechanisms is most predominant and which was the initiator of the deterioration process. A major limitation of microscopy is that it relies very much on the expertise and experience of the microscopist involved. However, when an experienced microscopist uses the method effectively, a wealth of information can be gathered, thus making it possible to diagnose the occurrence of deterioration processes in concrete. Sometimes, when used alone, the results obtained may not be conclusive. In such cases, it should be used as an integral part of an investigation, combined with other analyses. In most cases, when it is used as a first step in a series of analyses, it can eliminate unnecessary assumptions, because it enables the internal '*hidden*' structure and the composition of hardened concrete to be characterized.

8.7 Acknowledgement

This chapter benefited from the comments by M. R. de Rooij on a previous version.

8.8 References

ADAMS, A.E., MACKENZIE, W.S. and GUILFORD, C., 1984. *Atlas of sedimentary rocks under the microscope*. Longman, Harlow, 104 pp.

ADDIS, B.J. and OWENS, G., eds, 2001. *Fulton's concrete technology*. 8th rev. ed., Cement and Concrete Institute, Midrand, 330 pp.

ASTM C295, 1954 (revised 1998). *Standard guide for petrographic examination of aggregates for concrete*.

ASTM C457, 1960 (revised 2008). *Standard test method for microscopical determination of parameters of the air-void system in hardened concrete*.

BLOSS, F.D., 1994. *Crystallography and crystal chemistry*. 2nd ed., Mineralogical Society of America, Washington, 545 pp.

BONEN, D. and DIAMOND, S., 1994. Interpretation of compositional patterns found by quantitative energy dispersive x-ray analysis for cement paste constituents. *Journal of the American Ceramic Society* **77**:1875–1882.

BROCKEN, H. and NIJLAND, T.G., 2004. White efflorescence on brick masonry and concrete masonry blocks, with special emphasis on sulfate efflorescence on concrete blocks. *Construction and Building Materials* **18**:315–323.

CAMPBELL, D., 2004. Microscopical quality control of clinker and cement. In: Bhatty, J.I., Miller, F.M. and Kosmatka, S.H., eds, *Innovations in Portland cement manufacturing*. Portland Cement Association, Skokie, IL.

CARPENTER, A.B., CHALMERS, R.A., GARD, J.A., SPEAKMAN, L. and TAYLOR, H.F.W., 1966. Jennite, a new mineral. *American Mineralogist* **51**:56–74.

CHRISTENSEN, P., GUDMUNDSSON, H., THAULOW, N., DAMGARD-JENSEN, A.D. and CHATTERJI, S., 1979. Structural and ingredient analysis of concrete – methods, results and experience. *Nordisk Betong* **3**:4–9 (in Swedish).

CUR RECOMMENDATION 89, 2008. *Measures to prevent damage to concrete by alkali–silica reaction (ASR)*. 2nd rev. ed., CUR, Gouda, 48 pp.

CUR RECOMMENDATION 102, 2008. *Inspection and assessment of concrete structures in which the presence of ASR is expected or has been established*. CUR, Gouda, 31 pp.

DESCH, C.H., 1938. Henry Louis Le Chatelier. 1850–1936. Obituary Notices of Fellows of the Royal Society **2**(6):250–259.

DOLAR-MANTUANI, L., 1983. *Handbook of concrete aggregates, a petrographic and technological evaluation*. Noyes, Park Bridge, NJ, 345 pp.

ECKEL, E.C., 1928. *Cement, limes and plasters; their materials, manufacture and properties*. 3rd ed., reprinted 2005, Donhead, Shaftesbury, 699 pp.

FOX, J.M. and MILLER, P.T., 2007. The line method for petrographic determination of the quantity of fly ash and ground-granulated blast furnace slag in hardened concrete and blended cement. *Journal of ASTM International* **4**(1):9.

FRENCH, W.J., 1991. Concrete petrography: A review. *Quarterly Journal of Engineering Geology* **24**:17–48.

HANSEN, W.C., 1944. Studies relating to mechanism by which alkali–aggregate reaction produces expansion in concrete. *Journal of the American Concrete Institute* **15**:213–227.

HARTSHORN, S. and SIMS, I., 1998. Thaumasite, a brief guide for engineers. *Concrete* **32**(8):24–27.

HELLER, L. and TAYLOR, H.F.W., 1956. *Crystallographic data for the calcium silicates*. HMSO, London, 79 pp.

HEWLETT, P.C., ed., 1998. *Lea's chemistry of cement and concrete*. 4th ed., Arnold, London, 1053 pp.

HOBBS, D.W., 1988. *Alkali–silica reaction in concrete*. Thomas Telford, London, 183 pp.

HOWARTH, R.J., 1988. Improved estimators of uncertainty in proportions, point-counting, and pass-fail test results. *American Journal of Science* **298**:594–607.

JAKOBSEN, N.N., 1990. A microscopic study of sulphur concrete. In: *Proceedings of the 12th International Conference on Cement Microscopy*, Vancouver, 374–381.

JAKOBSEN, U.H. and BROWN, D.R., 2006. Reproducibility of w/c ratio determination from fluorescent impregnated thin sections. *Cement and Concrete Research* **36**:1527–1573.

JANA, D., 2005. Concrete petrography – past, present, and future. In: Hughes, J.J., Lesie, A.B. & Walsh, J.A., eds, *Proceedings of the 10th Euroseminar on Microscopy Applied to Building Materials*, Paisley.

JOHNSON, N.C., 1915. The microstructure of concretes. *Proceedings of the American Society of Testing Materials* **15**(II):171–213.

KATAYAMA, T., 2004. How to identify carbonate rock reactions in concrete. *Materials Characterization* **53**:85–104.

KLOES, J.A. VAN DER, 1924. *Onze bouwmaterialen. Deel III. Mortels en beton*. L.J. Veen, Amsterdam, 362 pp.

LARBI, J.A., 1997. Application of microscopy to the study of roof tile glazes: Case studies. In: *Proceedings of the 6th Euroseminar on Microscopy Applied to Building Materials*, Reykjavik, 70–80.

LARBI, J.A., 2004. Microscopy applied to the diagnosis of the deterioration of brick masonry. *Construction and Building Materials* **18**:299–307.

LARBI, J.A. and HEIJNEN, W.M.M., 1997. Determination of the cement content of five samples of hardened concrete by optical microscopy. *Heron* **42**:125–138.

LARBI, J.A. and NIJLAND, T.G., 2001. Assessment of fire-damaged concrete: Combining metamorphic petrology and concrete petrography. In: *Proceedings of the 8th Euroseminar* on Microscopy applied to Building Materials, Athens, 191–199.

LARBI, J.A. and VISSER, J.H.M., 1999. Diagnosis of chemical attack of concrete structures: the role of microscopy. *Proceedings of the 7th Euroseminar on Microscopy Applied to Building Materials*, Delft, 55–65.

LINDQVIST, J.E., NIJLAND, T., KONOW, T. VON, WESTER PLESSER, T.S., NYMAN, P., LARBI, J. and HEES, R. VAN, 2006. *Analysis of mortars with additives*. SP Swedish National Testing and Research Institute, Borås, SP Report 2006:06, 31 pp.

LORENZI, G., JENSEN, J. and WIGUM, B., 2006. Petrographic atlas of the potentially alkali-reactive rocks in Europe. EU PARTNER-project-GRD1-CT-2001-40103, 42 pp.

MACKENZIE, W.S., DONALDSON, C.H. and GUILFORD, C., 1982. *Atlas of igneous rocks and their textures*. Longman, Harlow, 148 pp.

MATHER, K., 1966. Petrographic examination of hardened concrete. In: *ASTM Symposium on Significance of Tests and Properties of Concrete and Concrete-making Materials*. ASTM 169a:125–143.

MIELENZ, R.C., 1962. Petrography applied to Portland cement concrete. In: Fluhr, T. and Legget, R.F., eds, *Reviews in Engineering Geology*. Geological Society of America, **1**:1–38.

NEVILLE, A.M. and BROOKS, J.J., 2001. *Concrete technology*. Rev. ed., Longman, Harlow, 438 pp.

NIJLAND, T.G. and LARBI, J.A., 2001. Unraveling the temperature distribution in fire-damaged concrete by means of PFM microscopy: Outline of the approach and review of potentially useful reactions. *Heron* **46**:253–264.

PARSONS, W.H. and INGSLEY, H., 1948. Aggregate reaction with cement alkalies. *Journal of the American Concrete Insitute* **19**:625–632.

PLAS, L. VAN DER and TOBI, A.C., 1965. A chart for judging the reliability of point counting results. *American Journal of Science* **263**:87–90.

POLDER, R.B. and LARBI, J.A., 1995. Investigation of concrete exposed to North Sea water submersion for 16 years. *Heron* **40**:31–56.

POLDER, R.P., NIJLAND, T.G., PEELEN, W. and BERTOLINI, L., 2002. Acid formation in the anode/concrete interface of activated titanium cathodic protection systems for reinforced concrete and the implications for service life. In: *Proceedings of the 15th International Corrosion Congress*, Granada, paper 97.

POTTS, P.J., BOWLES, J.F.W., REED, S.J.B. and CAVE, M.R., eds, 1995. *Microprobe techniques in the earth sciences*. Chapman & Hall, London, 419 pp.

RILEM TC 106-2, 2000. Detection of potential alkali-reactivity of aggregates – The ultra-accelerated mortar-bar test; *Materials and Structures* **33**:283–293.

RILEM TC 191-ARP, 2003. RILEM recommended test method AAR-1: Detection of potential alkali-reactivity of aggregates – Petrographic method. *Materials and Structures* **36**:480–496.

ROOIJ, M.R. DE and BIJEN, J.M.J.M., 1999. 'Active' thin sections. *Heron* **44**:79–90.

ROOIJ, M.R. DE, BIJEN, J.M.J.M. and FRENS, G., 1999. Active thin sections to study syneresis. *Cement and Concrete Research* **29**:281–285.

ROSSIKHINA, G.S., SHCHERBAKOVA, N.N., SHCHEDRIN, M.P., TOLUBAEVA, N.V. and BUKINA, T.F., 2007. Investigation of refractory concrete materials with aluminosilicate composition by petrographic methods. *Glass and Ceramics* **64**:404–407.

SHAYAN, A. and QUICK, G.W., 1991. Relative importance of deleterious reactions in concrete: Formation of AAR products and secondary ettringite. *Advances in Cement Research* **4**(16):149–157.

SIBBICK, R.G., CRAMMOND, N.J. and METCALF, D., 2003. The microscopical characterisation of thaumasite. *Cement and Concrete Composites* **25**:831–837.

SIMS, I. and BROWN, B., 1998. Concrete aggregates. In: Hewlett, P.C., ed., *Lea's chemistry of cement and concrete*. 4th ed., Arnold, London, 907–1016.

SORBY, H.C., 1858. On the microscopical structure of crystals, indicating the origin of minerals and rocks. *Quarterly Journal of the Geological Society* **14**:453–500.

STANTON, T.E., 1940. Expansion of concrete through reaction between cement and aggregate. *Proceedings of the American Society of Civil Engineers* **66**:1781–1788.

ST. JOHN, D., POOLE, A. and SIMS, I., 1998. *Concrete petrography, a handbook of investigative techniques*. Butterworth Heinemann, London, 488 pp.

STUTECH and STUFIB, 2006. Losse toplagen in monoliet afgewerkte betonvloeren – analyse van de oorzaak en aandachtspunten ter voorkoming. STUFIB, Nieuwegein, STUFIB-report 12.

SWENSON, E.G., 1957. A reactive aggregate undetected by ASTM tests. *ASTM Bulletin* **57**:48–51.

TAYLOR, H.F.W., 1998. *Cement chemistry*. 2nd ed., Thomas Telford, London, 459 pp.

TAYLOR, H.F.W., FAMY, C. and SCRIVENER, K.L., 2001. Delayed ettringite formation. *Cement and Concrete Research* **31**:683–693.

THOMAS, M., FOLLIARD, K., DRIMALAS, T. and RAMLOCHAN, T., 2008. Diagnosing delayed ettringite formation in concrete structures. *Cement and Concrete Research* **38**:841–847.

TÖRNEBOHM, A.E., 1897. The petrography of Portland cement. *Tonindustrie-Zeitung* **21**:1148–1150 and 1157–1159.

TRÖGER, W.E., 1982. *Optische Bestimmung der gesteinsbildenden Minerale. Teil 1. Bestimmungstabellen*. 5th ed., E., Schweizerbart'sche, Stuttgart, 188 pp.

WINCHELL, A.N., 1951. *Elements of optical mineralogy. Part II. Descriptions of minerals with special reference to their optical and microscopical characters*. 4th ed., John Wiley, New York, 551 pp.

YARDLEY, B.W., MACKENZIE, W.S. and GUILFORD, C., 1990. *Atlas of metamorphic rocks and their textures*. Longman, Harlow, 120 pp.